Dealumination mechanisms of zeolites and extra-framework aluminum confinement

Marius-Christian Silaghi, Céline Chizallet, Joachim Sauer, Pascal Raybaud

Demande d'autorisation de publication (D.A.P.)

(en application de la note de la Direction Générale du 1er septembre 2003)

1 - Partie réservée aux auteurs

DEMANDEUR* **(1ER AUTEUR IFP ENERGIES NOUVELLES) :** Chizallet **DATE :** 17/09/2015

TYPE DE PUBLICATION* : Article pour revue scientifique

CARACTERE DE LA PUBLICATION : rendant compte de travaux de recherche

TITRE* : Dealumination mechanisms of zeolites and extra-framework aluminum confinement

LISTE DES AUTEURS* (NOM, PRENOM, APPARTENANCE /SECTION POUR AUTEUR IFP ÉNERGIES NOUVELLES)

Marius-Christian Silaghi (R065), Céline Chizallet (R065), Joachim Sauer (Humboldt Univ. zu Berlin), Pascal Raybaud (R066)

TITRE DE LA REVUE / DU CONGRES* : Journal of Catalysis

(CONGRES : PRECISER SIGLE ET TITRE DEVELOPPE)

DATE PREVUE DE PARUTION / COMMUNICATION :

LIEU (VILLE- PAYS) / DATE(S) DU CONGRES* :

N° DE PROJET-ETUDE* : XDF15 001 **PROJET NTE * :** ☐ oui ☒ non

*** : champs obligatoires**

DEPOT DES ARTICLES DANS HAL-IFPEN : ARCHIVE OUVERTE INSTITUTIONNELLE D'IFPEN

Le demandeur autorise IFPEN à déposer son article dans HAL-IFPEN : ☒ oui (par défaut) ☐ non

Le demandeur a averti tous ses co-auteurs, y compris extérieurs, de la mise en dépôt de cette publication dans HAL-IFPEN ☒ oui (par défaut) ☐ non

NOM(S) : Chizallet **DATE :** 17/09/2015 **VISA(S) :** OK

---

2 - Avis du (ou des) directeur(s) concerné(s)

ACCORD SUR LE TEXTE DEFINITIF ☒ oui ☐ non Motif :

RESPECT DES CONSIGNES D'ECRITURE DES AFFILIATIONS AUTEURS ☒ oui ☐ non

Pour Rueil : IFP Energies nouvelles, 1 et 4 avenue de Bois-Préau, 92852 Rueil-Malmaison, France

Pour Solaize : IFP Energies nouvelles, Rond-point de l'échangeur de Solaize, BP 3, 69360 Solaize, France

NOM(S) : T. Cseri **DATE :** 17 septembre 2015 **VISA(S) :** ok

---

3 - Partie réservée au chef de projet

BREVETS ET PROTECTION DE L'EXPLOITATION INDUSTRIELLE	**oui**	**non**
Cette publication risque-t-elle de gêner : ▪ le dépôt de brevets ?	☐	☒
▪ les actions de développement industriel ?	☐	☒
▪ les relations commerciales avec un partenaire ou un client ?	☐	☒
o si oui lequel ? : (dans ce cas, renvoyer la D.A.P au CdR concerné, pour information)		

RESPECT DES OBLIGATIONS CONTRACTUELLES	**oui**	**non**
• Le travail a-t-il été conduit dans le cadre d'un contrat ?	☐	☒
• L'autorisation écrite des partenaires a-t-elle été obtenue ?	☐	☐

Nom des partenaires éventuels :

Décision du chef de projet : ☒ Accord ☐ Refus. Motif :

CHEF DE PROJET : Pascal Raybaud **DATE :** 17/9/15 **VISA(S) :** accord

4 – Après visa, veuillez faire parvenir cette D.A.P. sous format électronique à la Direction Scientifique (BasePublications) pour enregistrement, copie électronique à la Direction Juridique (Chantal Le Naour).

Pour tout renseignement concernant la saisie, adressez-vous à Françoise Bertrand poste 7190

5 – Après parution de votre publication (article, ouvrage, actes, résumé, poster, etc.), veuillez faire parvenir une copie complète de la version publiée, accompagnée de la page de titre du support et d'un résumé en français ou en anglais à la Direction Scientifique (BasePublications).

ATTENTION, si vous déverrouillez ce formulaire, vous perdrez le contenu des champs que vous aurez renseignés en lançant l'impression.

Dealumination mechanisms of zeolites and extra-framework aluminum confinement

Marius-Christian Silaghi,[1] *Céline Chizallet,*[1,*] *Joachim Sauer,*[2] *Pascal Raybaud*[1]

[1] IFP Energies nouvelles, Rond-point de l'échangeur de Solaize, BP3, 69360 Solaize, France

[2] Institute of Chemistry, Humboldt-Universität zu Berlin, Unter den Linden 6, 10099 Berlin, Germany

* Corresponding author, Tel: +33 4.37.70.22.42 ; Fax: +33 4.37.70.20.66

E-mail: celine.chizallet@ifpen.fr

silaghi@inorg.chem.ethz.ch ; celine.chizallet@ifpen.fr ; js@chemie.hu-berlin.de ; pascal.raybaud@ifpen.fr

Abstract

Dealumination of zeolites is a major issue in material science and catalysis for decades, with tremendous lack of knowledge about the molecular scale mechanisms involved. Considering four relevant zeolitic frameworks (MOR, FAU, MFI, CHA), we determine the formation mechanisms of extra-framework Al species (EFAL) $Al(OH)_3H_2O$ during dealumination, by using periodic density functional theory (DFT) calculations including dispersion corrections. We identify a rather universal mechanism based on water adsorption on the Al atom in anti-position to the Brønsted acid site allowing successive Al-O bond hydrolyses until dislodgement of the framework Al to a non-framework position. The determination of Brønsted-Evans-Polanyi (BEP) relationships for the entire dealumination pathway was possible, despite degradation of the correlation with increasing number of hydrolyzed Al-O bonds. Moreover, we quantify the confinement effect acting on EFAL species within the zeolites cavities and show that this effect is also a thermodynamic driving force for the Al extraction.

Keywords

Zeolite, dealumination, extra-framework aluminum, pentahedral aluminum, ZSM-5, SSZ-13, Faujasite, Mordenite, density functional theory

1. Introduction

Zeolites, crystalline alumino-silicate microporous materials possess interesting intrinsic and post-synthetic features, such as a strong acidity, resulting from Lewis- (LAS) and Brønsted-acid sites (BAS).[1, 2] Additionally their thermal robustness and well manageable pore sizes make them suitable candidates for industrial reactions such as fluid catalytic cracking, hydrocracking, isomerization and alkylation of various hydrocarbon molecules.[3-7] However, one major topic in zeolite synthesis lies within the tailoring of the shape, size and the connectivity of intra-framework channels[8-17] since confinement effects[18] and diffusion limitations can impose severe constraints on the reactants, intermediates and products.[19] Steam treatment of the zeolite is conducted to introduce mesopores,[20, 21] where by dint of Al-O and Si-O bond breakings a partial hydrolysis of the framework occurs. The removal of a certain number of hydroxylated Al or Si species from the framework leads to the formation of a moiety called silanol nest where four hydroxyl groups are expected to surround the tetrahedral void,[22, 23] even if the lifetime of such silanol nest is questioned.[24, 25] Such a silanol nest was also called hydrogarnet defect.[26] Recently Additionally, extra-framework aluminum (EFAL) and extra-framework silicon (EFSI), located within the cavities, are generated and studied extensively in literature.[20, 27-38] Several reports show that dealumination can be site specific.[36, 37, 39] In particular, NMR and FTIR analyses on steam treated H-Mordenite could reveal that Al is randomly distributed over 4 and 5 membered rings (MR) and that a favored dealumination of T3 and T4 sites, located in the 4MR takes place.[36, 37] At a mesoscopic scale, Weckhuysen *et al.* showed by focused ion beam (FIB) and scanning electron microscopy (SEM) that steaming treatment of ZSM-5 zeolite generates either surface mesoporosity (mild treatment) or uniformly distributed mesopores (severe treatment) where sinusoidal channels are more susceptible to the dealumination and hence mesopore formation compared to straight channels.[32, 40] On a

steamed NH_4-Y Agostini *et al.* were able to show that contrary to the general opinion the dealumination is not a high-temperature process but takes already place at moderate temperatures (450 – 500 K). They also show the appearance of 30-35% of the total Al within the sodalite cage.[28]

Considering the above mentioned experimental findings, one still misses *in situ* and *operando* approaches to reveal the atomic structure rearrangement occurring during the dealumination processes.[21] To gain atomistic insight into the mechanism, some early theoretical calculations have been used to describe both, the structure and catalytic properties of dealuminated zeolites in presence of EFAL species. Ruiz and co-workers for instance examined the structure and energetics of aluminum complexes serving as models for Brønsted-acid sites, without any explicit simulation of the zeolite framework.[41] Their results obtained by Hartree-Fock (HF) and Moller-Plesset second order perturbation theory (MP2) show that a transition from tetrahedral to octahedral Al occurs when the net charge of the cluster is q = +1.The latter is 7 kJ/mol lower in energy. In order to analyze the structure and coordination of some EFAL species (e.g. Al^{3+}, $Al(OH)_2^+$, $Al(OH)_3$), Bhering *et al.* used density functional theory (DFT) calculations on zeolite Faujasite,[30] modeled by a T_6 cluster, and showed that monovalent cations prefer a bi-coordination whereas di- and tri-valent cations are tetrahedrally coordinated with oxygen atoms near the framework aluminum. They also quantified the effect of EFAL on the Brønsted acidity.[42] Periodic DFT calculations were performed by Benco *et al.*[29] By analyzing the dynamical behavior of the EFAL species $(Al(OH)_3(H_2O)_3$ and $Al(OH)_3(H_2O)$ in Gmelinite, they revealed a localization depending mobility of these aluminum-hydroxide clusters. In the main channel, both, the two non-coordinated H_2O molecules and the EFAL are mobile, whereas a network of hydrogen bonds suppresses its mobility within the cage and the EFAL occludes the pore. They also

investigated the preferred location of the bare Al^{3+} ion as EFAL within a periodic Mordenite framework, and observed limited relaxation of the framework around this EFAL.[43]

Quantum mechanics / molecular modeling (QM/MM) calculations were performed to quantify the reaction energies for hydrolysis reactions in the surrounding of T sites substituted by various heteroatoms,[44, 45] but it is only very recently that full mechanisms were proposed from *ab initio* calculations to quantify both the thermodynamics and kinetics of zeolite hydrolysis reactions. The first periodic DFT calculations including thermodynamic and kinetic data and giving a first insight in the dealumination and desilication mechanism were indeed reported by Swang *et al.*[46, 47] Employing H-Chabazite (SSZ-13) as zeolitic model, they simulated the subsequent addition of four water molecules leading to the formation of a silanol nest and a an EFAL being $Al(OH)_3H_2O$. In the same spirit they analyzed the creation of an EFSI species $Si(OH)_4$. Their first step, water adsorption on the proton of a Brønsted site, is followed by the formation of a vicinal disilanol (Si_V species) with a relatively high energy barrier, $E^{‡}$=175 kJ/mol for the desilication, and $E^{‡}$=190 kJ/mol for the dealumination. The origin of the strong energy cost might result from the strain in the 2MR cycle of vicinal disilanols. Subsequently, and without addition of water, they suggested an inversion of the molecular environment around this penta-coordinated Si species leading to the first Al-O-Si bridge breaking. Again, this reaction exhibits an energy barrier of $E^{‡}$=150 kJ/mol and $E^{‡}$=175 kJ/mol for the desilication and dealumination, respectively. Subsequent hydrolysis steps by the successive addition of one water molecule at each step finally lead to the formation of an EFAL or EFSI and silanol nest.

Inspired by these pioneering DFT studies, recently we examined the reactivity of several T sites belonging to various zeolitic frameworks, i.e. MOR, FAU, MFI and CHA, by periodic calculations based on density functional theory (DFT) augmented with a dispersion term[48] (DFT+D2) which were supported by hybrid MP2:DFT+D2 calculations.[49] We found a

general pathway for the initiation of dealumination (first Al-O bond breaking, Figure 1-a), which consists in:

- water adsorption on the Al atom in anti-position to the Brønsted acid site, forming a penta- coordinated Al species (when the Al-O bond in anti to the water molecule remains, even if weakened) or tetra-coordinated Al species (when the Al-O bond in anti is broken), called I0($1H_2O$).
- a subsequent 1,2-dissociation of water on adjacent framework oxygen with axial substitution of the silanol group (in the case of a bipyramidal Al_V obtained upon adsorption of water in anti-position to the Brønsted acid site), leading to the I1($1H_2O$) intermediate. If the previous step did not break the Al-O bond in anti to the adsorbed water molecule, the present step leads to the first Al-O(H) bond breaking. Rotation of OH groups then occurs for a stronger hydrogen-bond network (I2($1H_2O$) species, Figure 1-a).

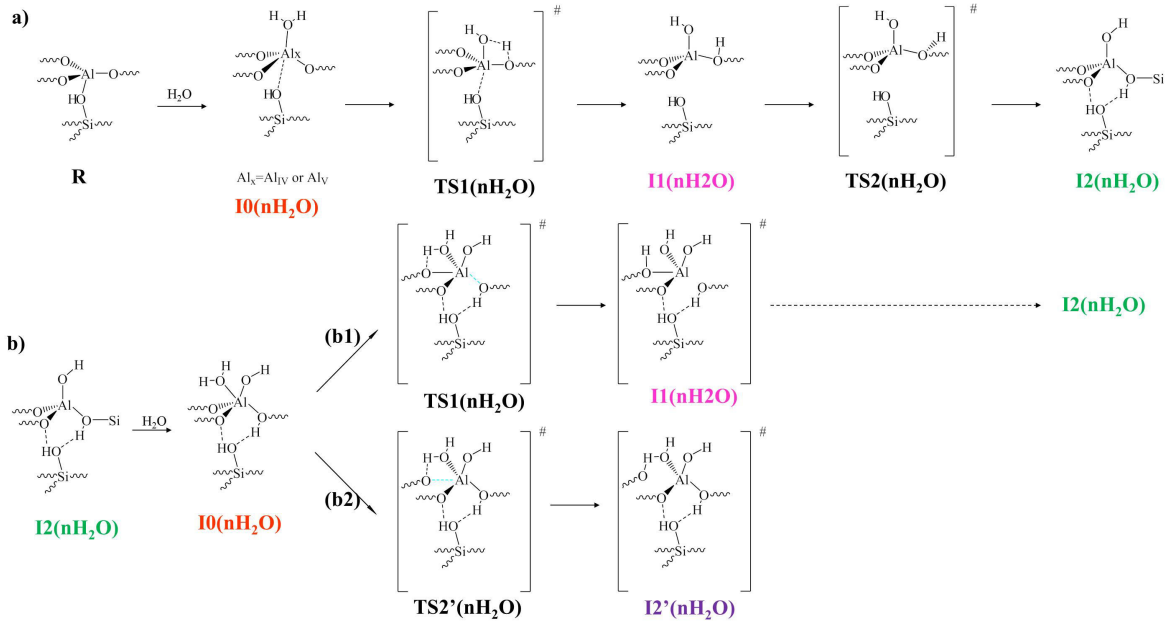

Figure 1. a) Anti attack of a water molecule (n = 1) on an Al atom in anti-position to the BAS (I0($1H_2O$)) followed by a 1,2-dissociation with axial substitution via a transition structure composed of a four membered ring (TS1($1H_2O$)) giving rise to I1($1H_2O$). Establishing a hydrogen bond between the newly created BAS and a silanol, via a proton rotation (TS2($1H_2O$)), leads to a more stable intermediate I2($1H_2O$). b) Anti attack of a water molecule (for n = 2) on an Al atom in anti position to the BAS (I0(nH_2O)) followed by: (b1) a 1,2-dissociation with axial substitution via a transition structure composed of a four membered ring (TS1(nH_2O)) leading to I1($2H_2O$), (b2) 1,2-dissociation with equatorial substitution via a transition structure composed of a four membered ring (TS2'($2H_2O$)) leading to I'2($2H_2O$). The difference between the (b1) and (b2) routes is the nature of the Al-O bond broken, depicted in light blue in the transition structures.

The energy barriers required are much lower than the ones reported earlier by Swang *et al*,[46] who recently showed that such mechanisms passing through water molecules adsorbed on Al atoms are also very relevant for the desilication of SAPO-34.[50, 51] Beyond that, we were able to generalize this initiation mechanism to the various sites of all zeolite frameworks investigated so far. We also revealed a Brønsted-Evans-Polanyi (BEP) relationship between the energy barrier relative to TS1 and the reaction energy to the first intermediate (I1). Based on the insight gained on the initiation of the dealumination process, here we address the propagation of Al-O bond breaking, up to the formation of EFAL. Does this mechanism discovered for the initiation step also apply to the subsequent elementary steps of the dealumination pathway? Do more favorable alternative pathways exist once the first Al-O bond is broken? How do the energy barriers evolve on the course of the dealumination pathway? Is there an impact of the zeolite framework on the mechanism and on the stability of the resulting EFAL? To answer these key questions, we report in the present work periodic DFT+D2 calculations, aiming at establishing the complete reaction path (intermediates and transition structures) for the genesis of EFAL at several sites of MOR, FAU, MFI and CHA. We investigate the specific case of $Al(OH)_3(H_2O)_4$ as EFAL species, resulting from the interaction of four water molecules with the Al site. Once the first Al-O bond is broken and the Al atom becomes more flexible in terms of structural changes, alternative pathways are investigated. We also look at Brønsted-Evans-Polanyi (BEP) relationships. Finally, we consider confinement effects on EFAL species within the zeolites cavities, with the aim to find out if the stability of the final dealumination product has an impact on the regioselectivity of dealumination.

2. Methods

2.1. Structure Optimization

Structure optimizations have been performed by the Vienna ab initio simulation package VASP.[52-54] A plane-wave basis set using the projector-augmented wave (PAW)[55] has been employed and the gradient corrected exchange correlation functional of Perdew, Burke and Ernzerhof[56] (PBE) is used. Moreover, a semiempirical $1/r^6$ term, parametrized by Grimme (D2),[48] is added to the PBE functional to account for dispersion forces (PBE+D2). We checked that energeties were correctly described by comparison with hybrid MP2:DFT+D2 calculations performed with QMPot[57, 58] (see ref. [49]). Van der Mynsbrugge *et al.* analyzed in detail[59] the reliability of different approaches (cluster, periodic boundary conditions) and functionals. They found that adsorption enthalpies of water, alcohols and nitriles, calculated by the PBE-D2 functional and applying periodic boundary conditions, are reasonably consistent with experimental data. Göltl et al. made the same observation for hydrocarbon adsorption in CHA.[60]

For cell optimizations on pure silica zeolites (including ionic positions and cell parameters), a 1x1x1 unit cell was used for FAU, CHA and MFI and a 1x1x2 unit cell for MOR. This latter has been done since the cell parameter c = 7.40 Å is too small to minimize the lateral between periodic images of the acid sites and the extra-framework species appearing during the demetallation. All calculations were performed at the Γ-point. The cutoff energy for the plane-wave basis is set to 800 eV for the full cell relaxation of siliceous zeolites. This setting avoids problems related to the incompleteness of the plane wave basis set with respect to volume variations (Pulay Stress). The obtained unit cell parameters (see Supporting Information S1) for the siliceous zeolites were kept unchanged after substitution of Al for an Si. Furthermore, a proton serving as counter ion was connected to a framework oxygen atom. For all further calculations, the cut-off energy is set to 400 eV. The electronic

optimizations were done up to a convergence of $1x10^{-6}$ eV for the self-consistent loop and until all forces on atoms are lower than 0.02 eV/Å. Reaction energies ΔE are defined according to equation 1.

$$\Delta E = E_{zeo\text{-}n(water)} - E_{zeo} - nE_{water} \quad (1)$$

with E_{zeo}, $E_{zeo\text{-}n(water)}$ and E_{water} being the energy of the zeolite, the adsorbed zeolite-n(water) system and the water molecule, respectively (n is the number of adsorbed water molecules per unit cell, thus per Al atom). Thus, the non-hydrated zeolite cell serves as reference for all calculations.

2.2. Localizing transition structures

Starting with the optimized initial and final structures, an initial reaction path comprising 8 or 16 images, depending on the complexity of the analyzed reaction, is created. For this either a linear interpolation or, for complex reactions, an interpolation scheme involving both Cartesian and internal coordinates was used, using the string method.[61] In the latter case, the software Opt'n Path developed by Paul Fleurat-Lessard[62] was employed. In a first attempt, a first Nudged Elastic Band (NEB) method run is carried out.[63] For this the cut-off energy is set to 400 eV and the electronic structure optimizations is conducted up to a convergence of $1x10^{-6}$ eV for the SCF cycle and until all forces are lower than 0.02 eV/Å per atom. Since generally, even a large number of ionic steps (~500) does not result in a converged reaction path, fulfilling the above mentioned criteria, the optimization is interrupted after 200 ionic steps. For some reactions, this approach is sufficient and the highest energy image is subsequently subjected to a quasi-Newton optimization algorithm[64] having the same convergence criteria as the NEB calculation, followed by a vibrational analysis in order to check the existence of only one negative frequency along the reaction coordinate. For this purpose, the same convergence criteria as for the NEB calculation have

been employed with a displacement of ±0.01 Å in each direction, in order to stay within the harmonic approximation. However, it is not possible to eliminate all but one imaginary frequency. Nevertheless, the residual spurious frequencies are very low and correspond to modes of the zeolitic framework without implication of the reaction center. For more complex reactions, where the transition structures could not be found by a first NEB run a subsequent NEB with 8 images between the two structures enclosing the supposed transition structure is carried out. For some specific cases where the combination of two NEB steps did not result in any satisfactory transition structures, an improved Dimer[65] calculation was performed after the first NEB run, starting from the highest energy point.

3. Results

3.1. Dealumination pathways including four H_2O molecules leading to an EFAL ($Al(OH)_3H_2O$)

In each case, four water molecules were taken into consideration and added successively to create one tetrahedral EFAL of the type $Al(OH)_3H_2O$ as well as a silanol nest, where four Si-OH groups surround the vacancy left behind by the removal of the aluminum atom. Some relevant structures discussed below are reported in Supporting Information S2, and their energies are given in Supporting Information S3.

3.1.1 Mordenite

The T4O4 site was chosen for the investigation of the dealumination in Mordenite (see Figure S1 in Supporting Information for the terminology of the sites). The aluminum atom is located in the wall of the 12MR. This T site was chosen according to experimental data of Müller *et al*. stating that the extent of dealumination increased with the number of Brønsted acid sites being in interaction with framework oxygen atoms[36] and of van Geem *et al*. showing that

the T sites located in the 4MR are the first to dealuminate.[37] We firstly transposed the mechanism found for the initiation of the reaction, as reported in our previous paper[49] which is an 1,2 dissociation with axial substitution. By axial substitution, we refer to the leaving group, i.e. the silanol in anti-position to the water molecule to which the Al atom is initially connected to the framework. Then, we investigated alternative mechanisms once the reaction is initiated (n>1, with n= number of reacting water molecules). For MOR, the relevant intermediates are depicted in Figure 2, the full energy diagram being plotted in Figure 3. Additional structures (in particular: transition structures) are given in Supporting Information S2.

Pathway where 1,2 dissociation with axial substitution occurs at each step

Since the importance of the first water attack on the aluminum atom has been described in detail in our previous paper[49], we only recall the underlying mechanism (Figure 1-a) and focus more on the evaluation of complete reaction path (Figures 2 and 3) leading to the extraction of an Al atom from the zeolitic framework to an extra-framework position.

1H_2O

The first water molecule is adsorbed (with ΔE = - 67 kJ/mol) on the Al T4 site via an Al-O(H_2) bond of 2.14 Å, and one short hydrogen bond (1.68 Å) with O4 atom. Water remains located in the 12MR in anti-position to the Brønsted acid site where the initial tetrahedral Al atom exhibits now pentahedral coordination. Upon adsorption, the Al-O(H) bond increases from 1.90 Å to 2.12 Å. Experimental analyses based on ^{27}Al MAS NMR suppose that penta-coordinated (trigonal bipyramidal) or tetra-coordinated (distorted tetrahedral) Al species are at the initiation of the aluminum dislodgement from the zeolitic framework.[28, 31] Subsequently the water molecule is split on an adjacent framework oxygen atom via a 1,2-dissociation with axial substitution (Figure 2). Surpassing a transition structure (TS1(1H_2O))

composed of a four membered ring ($E^{‡}$ = 100 kJ/mol) leads to intermediate I1(1H_2O) (ΔE = 26 kJ/mol). The first Al-O(H) bond is definitively broken since its length becomes 3.19 Å.

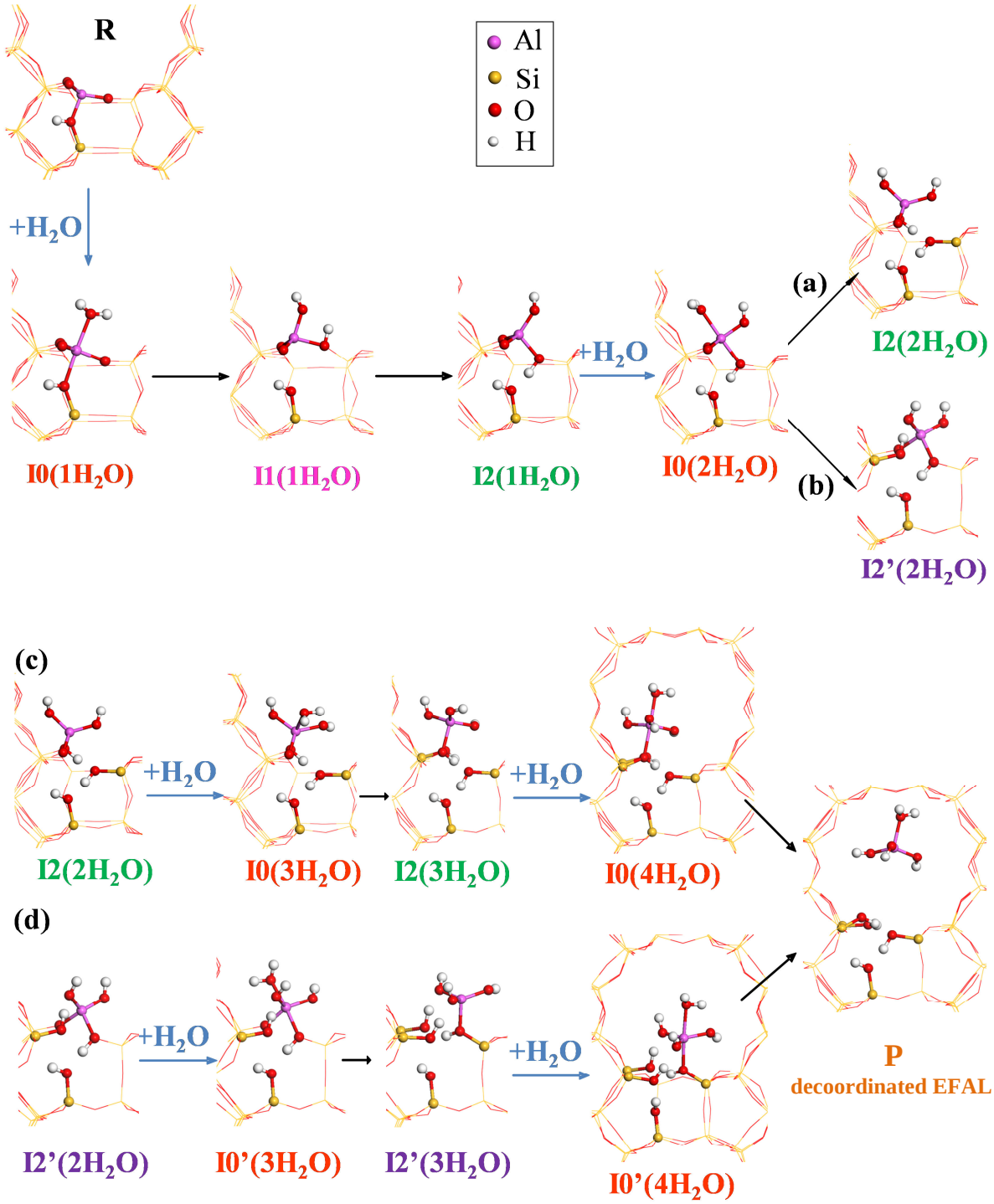

Figure 2. Reaction intermediates for EFAL formation starting from the T4O4 site in MOR. The terminology is the same as in figure 3, as well as the color code.(neither of them is given in Fig. 3, moreover, this type of info should be given in the first figure in which it appears) (a) 1,2-dissociation with axial substitution leading to I2(2H_2O), (b) 1,2-dissociation with equatorial substitution leading to I2'(2H_2O). (c) further transformation of I2(2H_2O), by 1,2-dissociation with axial substitution reactions, (d) further transformation of I2'(2H_2O), by 1,2-dissociation with equatorial substitution reactions. All corresponding TS structures are reported in Supplementary Information S2.

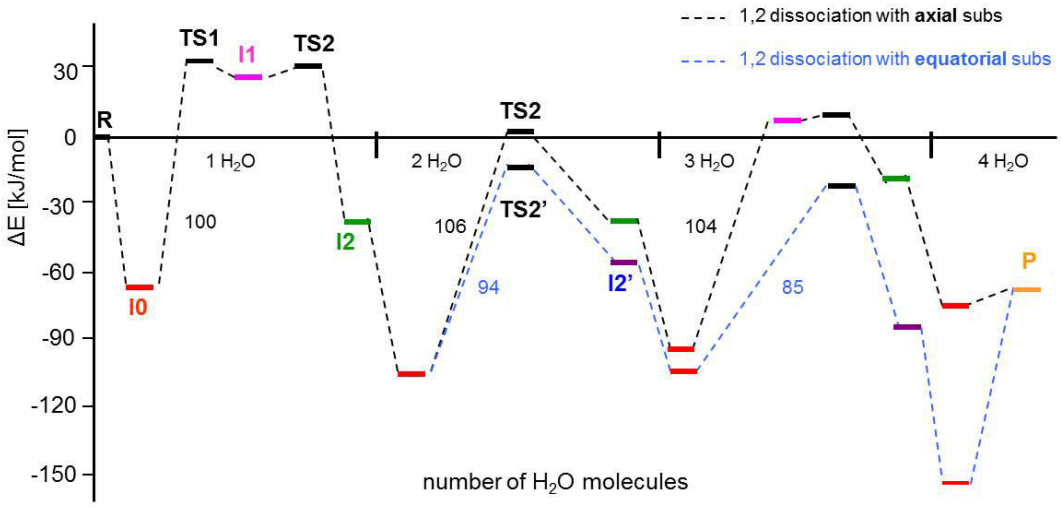

Figure 3. Energy profiles with energy barriers of the two possible dealumination pathways of the T4O4 site in H-MOR including four water molecules and leading to an EFAL $Al(OH)_3H_2O$. The structures of the relevant intermediates are reported in Figure 2, that of the transition structures in Supporting Information. For the sake of clarity, the number of water molecules was omitted in the name of intermediates and transition structures, but they are shown on the x-axis.

A weakly activated proton rotation of the newly created BAS ($E^{\ddagger}$ = 4 kJ/mol) gives rise to a more stable intermediate I2($1H_2O$) (ΔE = -38 kJ/mol) due to the presence of a hydrogen bond between the proton and the oxygen atom of the silanol group. The distance between the tetrahedrally coordinated pre-EFAL and the oxygen atom of the former BAS has increased further to 3.34 Å. Moreover, the partially dislodged pre-EFAL points towards the 12MR. With increasing amount of water, the pre-EFAL will become more flexible due to the decreasing number of Al-O bonds binding it to the framework.

In the present section, subsequent Al-O hydrolyses are considered to follow the same pattern, i.e. water adsorption on Al in anti-position to the BAS followed by a 1,2- dissociation of the water molecule with axial substitution and a rotation of the proton in order to establish a hydrogen bond with an oxygen atom of a silanol (Figure 1-b1).

$2H_2O$

Adsorption of the second water molecule on aluminum (ΔE = - 106 kJ/mol) leads to I0($2H_2O$) exhibiting a penta-coordinated Al with an increase of the second Al-O(H) bond (to be broken)

from 1.87 Å to 1.98 Å and an oxygen-aluminum bond between the water molecule and the framework aluminum of 2.13 Å. For the second Al-O hydrolysis, the analogous I1($2H_2O$) intermediate has not been identified while the TS2($2H_2O$) transition structure was found: the latter TS involves the Al-O bond breaking and the proton rotation at the same time. The corresponding reaction barrier for this Al-O bond breaking is as high as 106 kJ/mol, thus a value slightly higher than the one of the first step. It leads to I2($2H_2O$) (ΔE = -37 kJ/mol, very close to I2($1H_2O$)) with an Al-O bond length of 2.89 Å between the Al atom and the oxygen atom of the silanol.

$3H_2O$

A third water molecule is needed to enable the last Al-O hydrolysis giving rise to the an hydroxylated $Al(OH)_3$ EFAL species which is linked to the framework by one residual Si-O bond, I2($3H_2O$). Upon water adsorption on aluminum (ΔE = - 95 kJ/mol) the Al-O(H) bond in I0($3H_2O$) increases from 1.93 Å to 2.04 Å and leads to a trigonal bipyramidal coordinated EFAL precursor with an Al-O bond of 2.12 Å between the oxygen atom of the water molecule and the Al atom. A subsequent 1,2-dissociation of the water molecule results in the intermediate I1($3H_2O$) (ΔE = 7 kJ/mol). No TS1($3H_2O$) distinct from I1($3H_2O$) could have been identified but only TS2($3H_2O$) leading to I2($3H_2O$) (ΔE = - 20 kJ/mol). The effective energy cost required to form I1($3H_2O$) is $E^{\ddagger}$ = 104 kJ/mol (very close to the previous reaction barriers). The last Al-O bond is broken (3.49 Å) resulting in a trigonally planar $Al(OH)_3$ EFAL and a silanol nest composed of 4 silanol groups establishing hydrogen bonds with each other and the framework. The EFAL is still connected to one oxygen atom ($Al\text{-}O^{silanol}$ = 1.97 Å) of the silanol nest.

4H_2O

Although only three water molecules are needed to strongly displace the framework Al to a non-framework position a fourth molecule is adsorbed on Al in anti-position to the BAS (ΔE = - 76 kJ/mol) leading to a trigonal bipyramidal $Al(OH)_3H_2O$, $I0(3H_2O)$ intermediate, where the EFAL is still coordinated to the framework with $Al\text{-}O^{framework}$ and $Al\text{-}O^{water}$ bond lengths of 2.13 Å. In a last step, the EFAL is decoordinated (with Si-O bond breaking) giving rise to a tetrahedrally coordinated Al atom residing in the 12MR (ΔE = - 68 kJ/mol) with three Al-OH bonds of length 1.74 Å, 1.73 Å, 1.74 Å and one $Al\text{-}O^{water}$ bond of 1.96 Å. To evaluate the energy cost for this last step, the position of the decoordinated EFAL was constrained at the center of the 12MR channel such as interactions with the zeolitic framework are minimized. The corresponding energy cost is very modest (+8 kJ/mol) with an activation barrier of +25 kJ/mol. The EFAL stability is the subject of a more detailed study devoted to the confinement effect on EFAL species in section 3.3.

From this analysis achieved on the T4O4 site of Mordenite, it can be concluded that the transposition of the mechanism found as most favorable for the first Al-O bond breaking, (e.g. water molecule adsorption on Al in anti to the BAS, followed by 1,2 dissociation with axial substitution), leads to the formation of the EFAL species without significant change of energy barriers (100-106 kJ/mol) along the first 3 hydrolysis steps being thus equally kinetically limiting. The fourth hydrolysis step is far less energetically demanding than the others. However, in the course of our transition structure sampling, we found that an alternative pathway could be possible for n > 1, which is presented in the following paragraph.

Alternative pathway for n(H_2O) > 1 :1,2 dissociation with equatorial substitution

For water amounts n ≥ 2 and thus once the first Al-O bond is hydrolyzed, we found that a less activated reaction path is possible. The first step for the underlying mechanism for

$n(H_2O) \geq 2$ is still a water adsorption on Al in anti-position to the BAS. However, it is now followed by a 1,2 dissociation on an adjacent framework oxygen atom with equatorial substitution as shown in Figure 1-b2 and Figure 2. By equatorial, we refer to the bond which is broken in TS2', starting from the bipyramidal Al_V in $I0(nH_2O)$ (Figure 1). Energetics are compared with that of the previous mechanistic sequence in Figure 3.

It has to be stressed out that this mechanism is not applicable to the initiation of the first Al-O bond breaking (this was checked) due to the rigidity of the framework around the aluminum atom. Since it is connected through four Al-O bonds to the framework an equatorial displacement of Al, inducing adjacent structural constraints, e.g. O-Si-O bond angles, this alternative mechanism is not possible and hence only an axial substitution for the first Al-O hydrolysis can be envisaged.

$2H_2O$

The aluminum-water complex $I0(2H_2O)$ serving as starting point for the second Al-O hydrolysis is the same as for the 1,2 dissociation with axial substitution (adsorption of the water molecule in anti to the newly formed BAS). A subsequent water splitting on an adjacent framework oxygen atom with equatorial substitution via $TS2'(2H_2O)$ ($E^{\ddagger}$ = 94 kJ/mol) leads to $I2'(2H_2O)$ with ΔE = -56 kJ/mol. At the same time, the involved Al-O bond increased from 1.77 Å to 3.26 Å depicting the second hydrolysis between the pre-EFAL and the framework. Comparing $I2(2H_2O)$ with $I2'(2H_2O)$, the latter product is about 20 kJ/mol more stable due to a hydrogen bond with a more polarized oxygen atom of the hydroxyl group of the EFAL precursor compared to the oxygen atom of the silanol group. The energy difference between TS2 and TS2' has a similar value of 22 kJ/mol, suggesting that a Brønsted-Evans-Polanyi (BEP) relationship may exist.

3H_2O

Water adsorption on Al (ΔE = -109 kJ/mol) increases the Al-O(H) bond from 1.87 Å to 1.98 Å resulting in a trigonal bipyramidal aluminum complex with a second apical Al-O^{water} distances of 2.13 Å. By a subsequent water splitting on the last adjacent framework oxygen atom holding the EFAL precursor coordinated to the framework ($E^{‡}$ = 85 kJ/mol for TS2'(3H_2O)) the Al atom is dislodged from a framework to a non-framework position in I2'(3H_2O) (ΔE = -86 kJ/mol). Here again, the kinetics of this mechanism with respect to the previous one seem to be driven by the thermodynamic as expected from BEP concept.

However, as in the preceding mechanistic approach the $Al(OH)_3$ species is not yet decoordinated from the zeolitic framework but remains bounded to a silanol (Al-$O^{silanol}$ = 1.93 Å). At this stage, two observations can be made : (i) the reaction barriers for the 1,2 dissociation with equatorial substitution compared to a 1,2 dissociation with axial substitution decrease with increasing amount of water and (ii) a stronger stabilization of I2'(nH_2O) compared to I2(nH_2O). Both thermodynamic and kinetic effects are thus connected by BEP relationship and are likely related to supplementary hydrogen bonds between the proton of a silanol and the oxygen atom of an hydroxyl group of the EFAL-precursor and the final EFAL, which are absent during the 1,2-dissociation with axial substitution.

4H_2O

Due to the interaction of the EFAL species $Al(OH)_3$ with an oxygen atom of a silanol the adsorption of a fourth water molecule (ΔE = - 154 kJ/mol) leads to a penta-coordinated hydroxy-aluminate with apical Al-$O^{framework}$ and Al-O^{water} bond lengths of 2.06 Å and 2.13 Å, respectively. Decoordination of $Al(OH)_3H_2O$ leads to the same finale state as for the 1,2-dissociation with axial substitution. However, due to the significantly stronger stabilization of I0'(4H_2O) induced by supplementary hydrogen bonds and stronger Al-$O^{framework}$ bond, this last step is more energetically demanding (ΔE= 78 kJ/mol)) than for the previous mechanism.

In the framework of this alternative pathway, barriers are lower for $n \geq 2$ than in the previous one except for the very last decoordination step, and the first step becomes the rate limiting step of the overall EFAL formation. At this stage, it remains difficult to conclude which one of the two mechanisms is preferentially followed in MOR. The additional energy barrier for the decoordination step compensates the more favorable kinetic and thermodynamic parameters of the previous steps.

Because a detailed description for the 1,2 dissociation with axial or equatorial substitution was conducted in Mordenite and the underlying mechanism is transposable to the other T sites of other zeolites included in our study, we will detail in the following the most favorable pathway allowing a combination of both mechanisms in the course of dealumination.

3.1.2 Chabazite

The Chabazite structure contains only one inequivalent tetrahedral site, with four different oxygen positions giving four possible Brønsted acid site configurations (Supporting information S1). For our mechanistic investigation, we chose the T1O3 site, where the proton resides on an oxygen atom belonging to two four-membered and one six-membered ring. Contrary to the other three proton positions that are all part of the 8MR window, the proton at O3 can interact via intrazeolite hydrogen bonds (2.22 Å, 2.62 Å, 3.19 Å) with oxygen atoms of a six-membered ring. This choice was inspired by experimental findings obtained on other zeolites (MFI, Beta, Mordenite) for which it was proposed by dint of ^{1}H-NMR spectra that the extent of dealumination increased with the number of Brønsted acid sites being in interaction with framework oxygen atoms.[36] Figure 4-a reports the energy diagram discussed in the following.

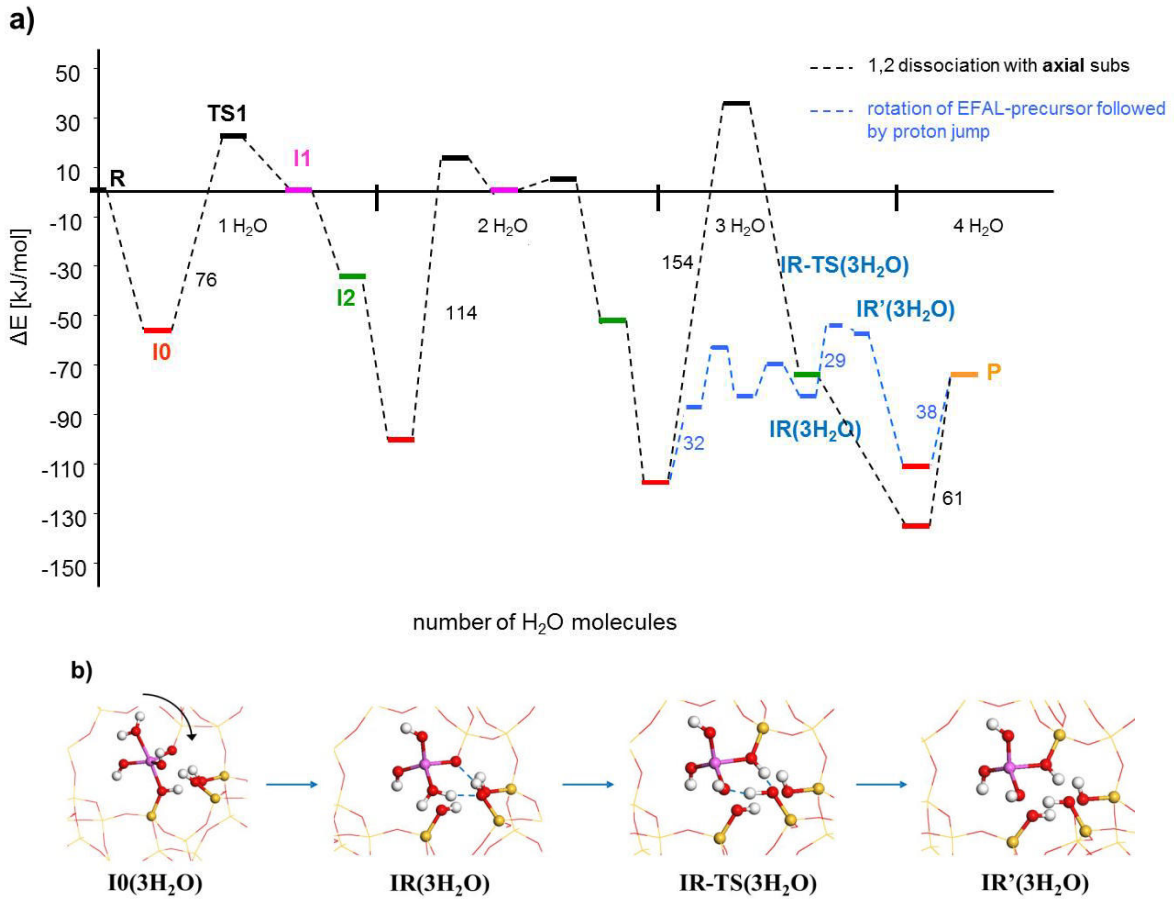

Figure 4. a) Energy profiles and energy barriers of the dealumination pathway of the T1O3 site in H-CHA including four water molecules and leading to an EFAL $Al(OH)_3H_2O$. b) Reaction pathway at T1O3 in H-CHA at $3H_2O$. The pre-EFAL undergoes a 90° rotation followed by a concerted proton jump leading to the formation of an $Al(OH)_3$ (pink: Al; red: Si; yellow: O; pink: Al; white: H). Blue dashed lines depict directions of O-H bond formation and breaking.

Preferred pathway for n(H_2O)=1 and 2 : 1,2 dissociation with axial substitution

The initiation of the first Al-O bond breaking again takes place via a 1,2-dissociation of the water molecule adsorbed in anti-position to the BAS, with axial substitution, as for Mordenite. In the case of Chabazite, this results in the lowest reaction barrier ($E^{\ddagger}$ = 76 kJ/mol) found for all our investigated T sites.[46, 47] Despite hardly predictable local structure effects (e.g. T-O-T angles) occurring during the dealumination process and hence making structure-activity relationship difficult to anticipate, a possible explanation for this low activation barrier might be the presence of an intra-zeolite hydrogen bond, with a more polarized framework oxygen atom bond to the Al atom. While the latter is absent for the T4O4 site in

H-MOR, its presence at T1O3 in H-CHA tends to stabilize TS1. In addition, this trend follows the BEP relationship between TS1($1H_2O$) and I1($1H_2O$).[49]

Contrary to the second Al-O bond breaking at T4O4 in H-MOR, which takes place via a 1,2-dissociation with equatorial substitution, at T1O3 in H-CHA a 1,2-dissociation with axial substitution is still the preferred pathway. As discussed for MOR, this might result from the local structure occurring during the dealumination process and hence the resulting intra-zeolite hydrogen bond network. At I2($2H_2O$) (ΔE = - 52 kJ/mol) three hydrogen bonds exist between a proton and an oxygen atom of (i) a silanol, (ii) a hydroxyl group of the EFAL precursor and (iii) the framework bound to the Al atom.

Alternative pathway for n(H_2O) > 2: occurrence of proton jumps

$3H_2O$

Transposing the two previous reaction mechanisms on the third Al-O bond breaking, via 1,2-dissociation with equatorial or axial substitution, did not lead to the identification of an I2'($3H_2O$). In addition, to form the intermediate I2($3H_2O$) , a relatively high reaction barrier of $E^{\ddagger}$ = 154 kJ/mol for TS2($3H_2O$) has to be overcome in order to give rise to an EFAL species of the form $Al(OH)_3$. However, this kinetically unfavoured reaction path can be bypassed due to the local configuration of the EFAL precursor still attached to the framework and the resulting silanol nest upon partial dealumination. In I3(H_2O) the precursor can undergo a 90° rotation around one Al-O bond axis keeping the EFAL precursor attached to the framework (IR($3H_2O$), Figure 4-b) so that a proton of the initially adsorbed water molecule on Al can establish a hydrogen bond with an oxygen atom of a silanol, and at the same time the proton of the silanol group displays a hydrogen bond with a framework oxygen atom attached to Al. The first step of this process is an Al-O(H) bond breaking ($E^{\ddagger}$ = 32 kJ/mol, Figure 4-b) followed by a rotational movement of the EFAL precursor along the Al-O axis leading to the intermediate described above. This is followed by a concerted proton jump

$H^{water} \rightarrow O^{silanol} // H^{silanol} \rightarrow O^{framework}$ ($E^{\ddagger}$ = 29 kJ/mol, IR-TS($3H_2O$)) leading to an $Al(OH)_3$ adsorbed on an oxygen atom of a silanol ($Al\text{-}O^{silanol}$ = 1.93 Å).

4H_2O

As for the case of Mordenite, due to the coordinated EFAL species on a silanol, a fourth water adsorption (ΔE = - 112 kJ/mol) results in a penta-coordinated hydroxy-aluminate with apical $Al\text{-}O^{framework}$ and $Al\text{-}O^{water}$ bond lengths of 2.11 Å and 2.12 Å, respectively.

In summary for Chabazite, an alternative route can lead to significantly lower barriers to be overcome for high hydroxyl content. However, the rate limiting step is the second Al-O dissociation ($E^{\ddagger}$ =114 kJ/mol), with a barrier higher than in MOR, whereas the first one is moderately activated as compared to MOR (and other zeolites as described subsequently). As previously discussed in for the initial step of the first Al-O bond breaking,[49] we confirm that the overall mechanism proposed here on the basis of the water anti addition is more favorable from an energetic point view (energy barriers) than the previous one proposed in the literature.[46, 47]

3.1.3 MFI

The T sites chosen for the mechanistic investigation in MFI type zeolite is based on experimental findings by Karwacki *et al.* showing by dint of FIB and SEM analyses on steamed ZSM-5 that sinusoidal channels are more susceptible to the dealumination than straight channels.[32] Therefore, we envisaged the following T sites as representative examples (Figure S1):

- T3O4: located in the intersection region between sinusoidal and straight channels. On this T site, the BAS proton points in a small cavity displaying intra-zeolite hydrogen bonds with one oxygen atom bound to the Al (2.18 Å) and two framework oxygen atoms (2.37 Å, 2.97 Å).

- T10O2: located in the sinusoidal channels. The proton at T10O2 displays only one intra-zeolite hydrogen bond with a framework oxygen atom of length 1.70 Å.

- T11O3: located in the straight channel. The proton at this T site is in interaction via a hydrogen bond with two framework oxygen atoms of length 1.89 Å and 2.36 Å.

Figure 5 summarizes the reaction paths of these three T sites, where the envisaged mechanism for the EFAL formation is a 1,2-dissociation with axial substitution for the first Al-O bond breaking and for the subsequent ones a 1,2-dissociation with equatorial substitution, which exhibit the most favorable intermediates and transition structures. In what follows, we explain the main observed differences between the three sites, occurring along the pathway, and do not give a detailed mechanistic description for each step which has already been done for Mordenite and is transferable to the MFI framework.

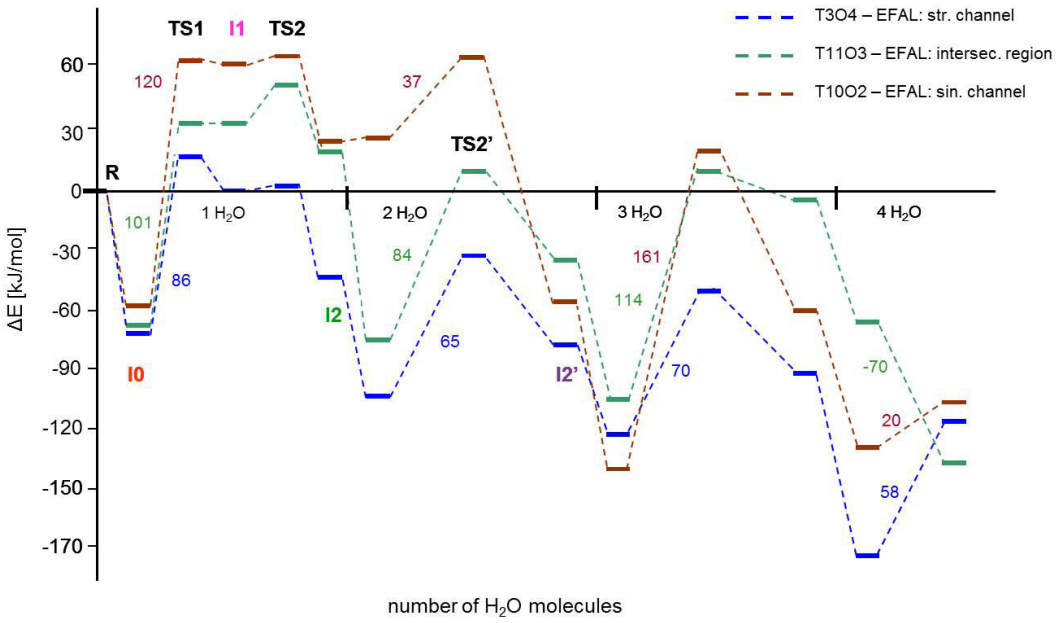

Figure 5. Energy profiles and energy barriers for the preferred dealumination pathway of the of the T3O4 (intersection between straight and sinusoidal channels), T10O2 (sinusoidal channel) and T11O3 (straight channel) site in H-MFI including four water molecules and leading to an EFAL $Al(OH)_3H_2O$.

1H_2O

Upon water adsorption, small differences (ΔE ~ 10 kJ/mol) in the adsorption energy are observed. The strongest adsorption is observed for T3O4 (ΔE = -70 kJ/mol, Figure 5) which is explained by an intra-zeolite hydrogen bond with a framework oxygen atom linked to Al and two hydrogen bonds established between the water molecule and two framework oxygen atoms in close vicinity (2.48 Å, 2.34 Å) as illustrated in Figure 6a). In contrast, a more pronounced energetic difference is observed for the first Al-O bond breaking and the resulting intermediates I1(H_2O) as well as the corresponding reaction barriers. Taking the T site T10O2 as an illustrative example, in the resulting penta-coordinated Al atom after water adsorption in anti-position, a strong hydrogen bond between a proton of the water molecule and a framework oxygen atom is formed (1.76 Å, Figure 6-a).

Such a short hydrogen bond is absent in the other two T sites. Moreover, the proton located on T10O2 is the one being split on an adjacent framework oxygen atom to initiate the first Al-O hydrolysis and thus explaining the highest activation barrier due to the energy needed to break this hydrogen bond. Additionally, the reaction barrier and the stability of I1(H_2O) are dictated by hydrogen bonds between the proton of the silanol (leaving group) and an oxygen atom linked to Al. This feature as well as the absence of a strong hydrogen bond upon water adsorption between the water molecule and framework oxygen atoms explain the lowest reaction barrier and highest stability of I1(H_2O) for the T3O4 site.

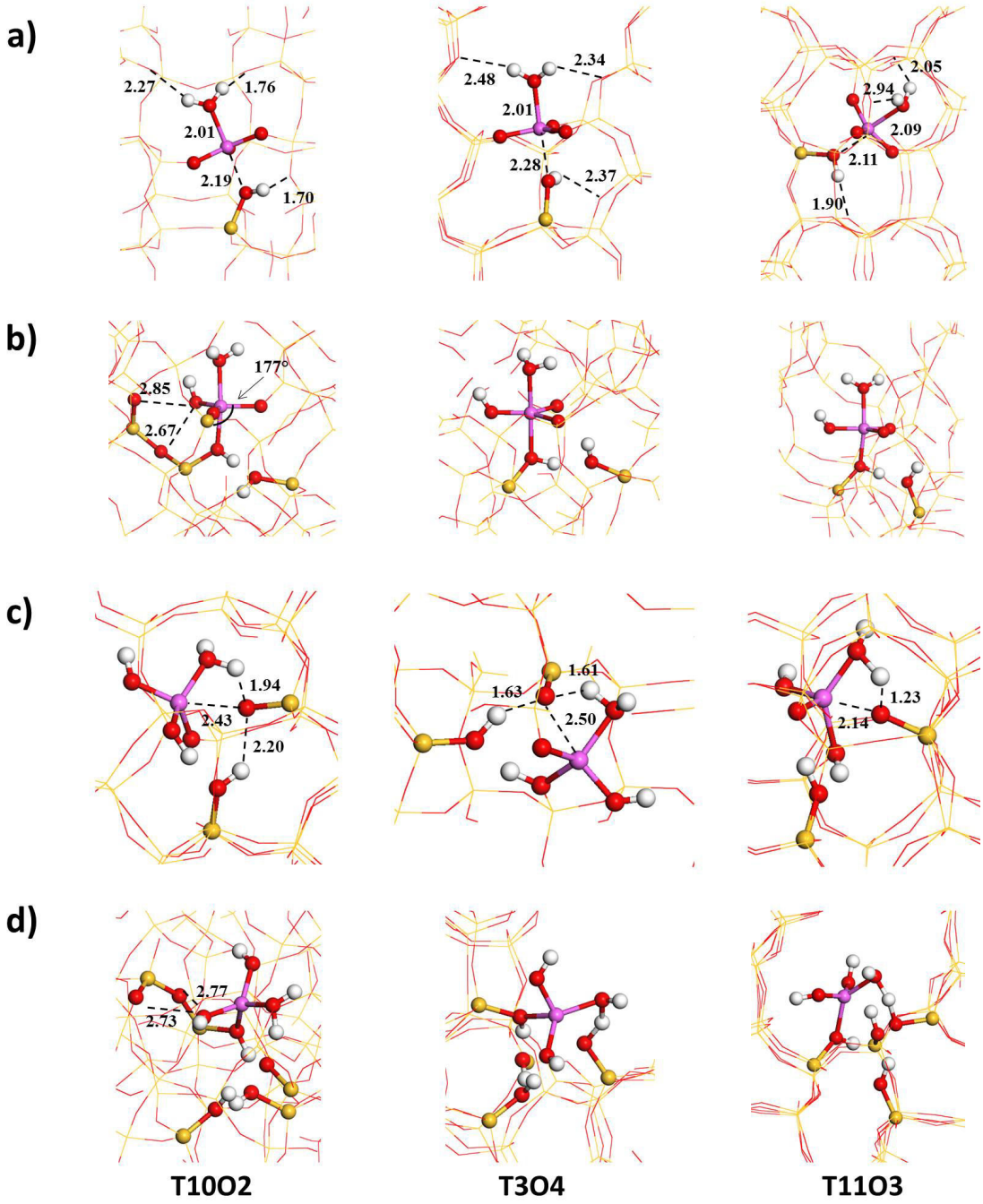

Figure 6. a) Water adsorption on Al in anti-position to BAS I0($1H_2O$), b) structures of I0($2H_2O$), c) corresponding transition structures TS2'($2H_2O$) and d) transition structures TS2'($3H_2O$) in MFI type zeolite at T10O2 (sinusoidal channel), T3O4 (intersection region) and T11O3 (straight channel). Bond lengths given in Å (pink: Al; red: Si; yellow: O; pink: Al; white: H).

$2H_2O$

Despite the presence of two hydrogen bonds (1.71 Å, 2.05 Å) between the water molecule and framework oxygen atoms, water adsorption at the T10O2 site is athermic which was only observed for this particular site (ΔE = 0 kJ/mol), whereas the T3O4 and T11O3 sites display

strong adsorption energies of ΔE = -54 kJ/mol and ΔE = -97 kJ/mol, respectively, resulting in very favorable I2($2H_2O$) intermediates. This illustrates the complexity in predicting the stability of intermediate species formed during the dealumination. Two reasons explain this result (i) a very unusual Al-O-Si angle of 177° with a Si atom as nearest neighbor which results from the water adsorption on Al and (ii) the constrained EFAL precursor induced by the local zeolitic framework, i.e. the hydroxyl group of the precursor displays two $O^{hydroxyl}$-$O^{framework}$ interactions of 2.85 Å and 2.67 Å which are the shortest found amongst all intermediates (Figure 6 b)). These are most certainly the major effects which destabilize the EFAL precursor at the T10O2 site compared to the two other I0($2H_2O$) intermediates.

In the subsequent Al-O hydrolysis steps, the T10O2 site passes through a highly instable transition structure compared to the T3O4 and T11O3 sites which is explained by the local structure of TS2'($2H_2O$). Two short hydrogen bonds of 1.61 Å and 1.63 Å at T3O4 and one hydrogen bond of 1.23 Å at T11O3 stabilize the transition structure, i.e. the silanolate, at these two sites. At T10O2 such stabilization is not achieved, due to the two significantly weaker hydrogen bonds of 1.94 Å and 2.20 Å, resulting in a highly unstable transition structure (Figure 5). However, once the local constraints at T10O2 –present since the adsorption of the second water molecule and in TS2'($2H_2O$) – relax, all three intermediates I2'($2H_2O$) result in energetically comparable structures.

3H_2O

The strongest adsorption is found for T10O2 (ΔE = -140 kJ/mol) in the series of these three T sites displaying hydrogen bonds with two framework oxygen atoms of length 2.54 Å and 2.19 Å. As for the second Al-O bond breaking, at T10O2 the stronger bonded proton is the one being transferred to an adjacent framework oxygen atom and thus explaining partially the high activation barrier. Additionally, in TS2'($3H_2O$) a hydroxyl group of the EFAL precursor

comes in close proximity with two framework oxygen atoms with $O^{hydroxyl}$-$O^{framework}$ interactions of 2.73 Å and 2.77 Å. As this short oxygen-oxygen interaction (presumably repulsive) is absent in TS2'($3H_2O$) on T3O4 and T11O3, the corresponding activation barrier are lower than for T10O2 (Figure 6 d)).

4$\underline{H_2O}$

Upon the exothermic adsorption of the fourth water molecule, a penta-coordinated $Al(OH)_3H_2O$ still in interaction with an oxygen atom of a silanol group is formed. In this last step, the decoordination of the EFAL species reveals either endothermic values or exothermic ones depending on the sites but they are not kinetically determining.

According to our analysis, it appears that the T3O4 site located at the intersection of straight and sinusoidal channels exhibits the smallest energy barriers ($E^{\ddagger}$=86 kJ/mol) whereas T10O2 located in the sinusoidal ones exhibit the highest ones ($E^{\ddagger}$=161 kJ/mol). T11O3 reveals an intermediate profile ($E^{\ddagger}$=114 kJ/mol). This result thus confirms the regioselectivity observed for the initial activation step (n = 1, see reference [49]), so that we can expect that dealumination is sensitive to the site location.

3.1.4 FAU

The framework of Faujasite contains only one inequivalent T site resulting in four proton positions. According to Neutron Powder Diffraction studies of D-Y and H-Y zeolite samples Czjzek *et al.* found the preferred proton positions for the O1 and O3 site where the highest occupation of protons was at the O1 site.[66] These proton sites were then considered in our mechanistic investigation. The proton bound to O1 points in to the super cage and displays an hydrogen bond with an oxygen atom linked to Al (2.34 Å), it will lead to an

EFAL in the sodalite cage. Symmetrically, the proton located at O3 is oriented towards the hexagonal prism and in interaction with two framework oxygen atoms (2.62 Å, 2.59 Å) and will lead to an EFAL in the supercage. Figure 7 compares the energy profiles for the preferred pathways found for these two T sites.

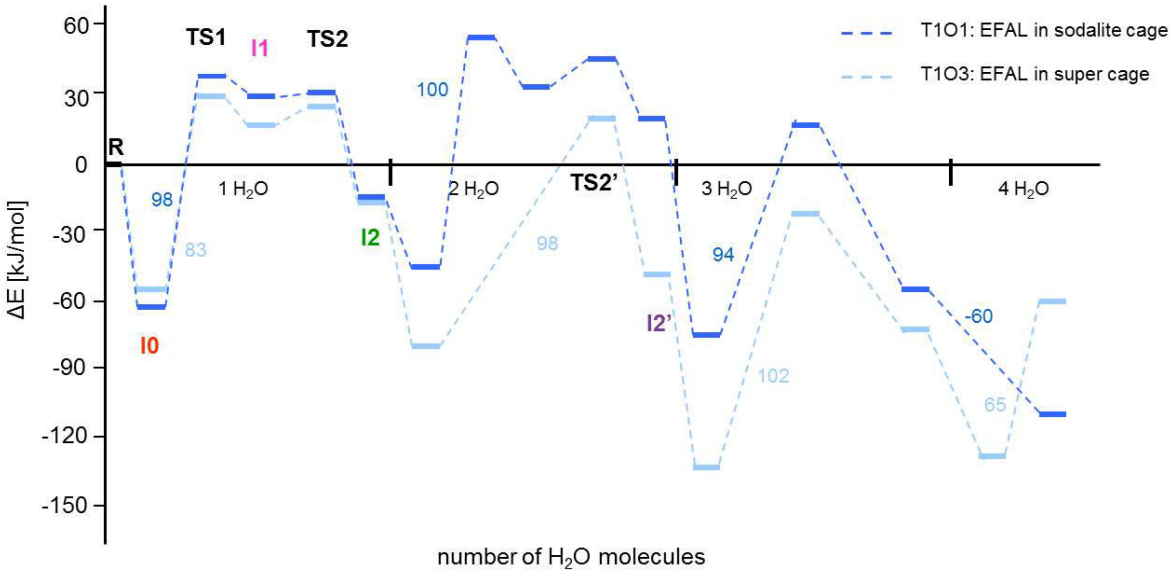

Figure 7. Energy profiles and energy barriers along the dealumination pathways of the T1O3 and T1O3 site in H-FAU including four water molecules and leading to an EFAL $Al(OH)_3H_2O$.

1H_2O

As for the previous zeolites, after water adsorption on Al in anti-position to the BAS, the first Al-O bond breaking takes place via a 1,2-dissociation of the water molecule with axial substitution. The corresponding energy barriers are 83 kJ/mol and 98 kJ/mol for the T1O3 and T1O1 sites respectively, which are in the same order of magnitude as the other investigated T sites. Again, the small differences between the intermediates and transition structures result from the interplay with a different hydrogen bond network occurring during hydrolysis.

2H_2O

The differences in the adsorption energies of T1O1 (ΔE = -45 kJ/mol) and T1O3 (ΔE = -79 kJ/mol) upon the second water adsorption is again due to the different local hydrogen bond network and the topology of the two initial oxygen positions. While in the

case of T1O1 the water attack on Al in anti-position takes place in the sodalite cage, for T1O3 the water molecule is located in the super cage upon adsorption on Al. However, upon hydrolysis of the second Al-O bond the mechanisms differ. While the reaction on the T1O1 site takes place via a 1,2-dissociation with axial substitution ($E^{\ddagger}$ = 100 kJ/mol), the preferred mechanism for the T1O3 site is via a 1,2-dissociation with equatorial substitution ($E^{\ddagger}$ = 98 kJ/mol). At this stage it is important to know, that the second Al-O bond breaking on T1O1 is also possible via a 1,2-dissociation with equatorial substitution ($\Delta E(I2'(2H_2O))$ = -8 kJ/mol, data not shown) however the corresponding reaction barrier is at about $E^{\ddagger}$ = 130 kJ/mol and thus, based on the kinetics of the reaction this pathway was not further considered.

3H_2O

Upon water adsorption in anti-position a pentahedral Al species is formed with ΔE = -74 kJ/mol and ΔE = -128 kJ/mol for the T1O1 and T1O3 site, respectively. In the subsequent and last Al-O hydrolysis leading to an EFAL $Al(OH)_3$ the reaction pathways of both T sites occurs via a 1,2-dissociation with equatorial substitution and with an activation barrier of 94 kJ/mol for the T1O1 site and 102 kJ/mol for the T1O3 site. In both cases, this leads to an EFAL $Al(OH)_3$ which is still linked to an oxygen atom of a silanol, and located either in the supercage for T1O3 (ΔE = -72 kJ/mol) or in the sodalite cage for T1O1 (ΔE = -54 kJ/mol).

4H_2O

Adsorption of the forth water molecule on Al in anti-position leads in the case of T1O3 to a penta-coordinated EFAL species (ΔE = -125 kJ/mol) which is still coordinated to one oxygen atom of a silanol group (1.91 Å). After a last bond breaking, it becomes an $Al_{IV}(OH)_3H_2O$ and resides in the supercage (ΔE = -60 kJ/mol). For T1O1, the EFAL spontaneously leaves the

silanol nest upon the fourth water adsorption on Al: this phenomenon is only observed for this particular T site. The EFAL resides in the center of the sodalite cage establishing a network of multiple hydrogen bonds with framework oxygen atoms (as discussed later).

3.1.5. Synopsis

By a systematic determination of the dealumination pathways occurring in zeolites FAU, MOR, MFI and CHA (with high Si/Al), we are now able to provide insights into the molecular scale's mechanisms. We have revealed for the first time the universal feature of the water adsorption on Al in anti-position to BAS leading to the formation of pentahedral or distorted tetrahedral aluminum species and activating the dealumination process. These species are at the initial stage before each Al-O hydrolysis and are subsequently transformed into a tetrahedral species. Whereas for the first Al-O bond breaking this hydrolysis takes place uniquely via a 1,2-dissociation with axial substitution, the mechanisms for the following steps display a heterogeneity due to local structure effects which are difficult to anticipate without DFT calculations. Once the first Al-O bond is broken the EFAL precursor becomes more flexible in the framework in terms of structural constraints leading to one main alternative dealumination pathways (Table 1) such as 1,2-dissociation with equatorial substitution. Another possible path was identified in CHA where the rotation of the EFAL precursor followed by a concerted proton jump was revealed. A careful analysis of the intermediates and transition structures occurring along the dealumination pathway showed that this results from the different T site location within the zeolitic framework and from hardly predictable interactions (mostly hydrogen bonds) between the pre-EFAL and the zeolite's wall. Table 1 highlights this regioselectivity and the fact, that the first Al-O bond breaking step is not always determining for the formation of EFAL, when considering intrinsic energy barriers. The regioselectivity is often linked to the Al-O breaking propagation mechanism. Whereas for

the T4O4 site in Mordenite the rate limiting step is dictated by the first Al-O bond breaking ($E^{\ddagger}$ = 100 kJ/mol) via 1,2-dissociation with axial substitution, the rate limiting step for the T11O3 site in MFI ($E^{\ddagger}$ = 100 kJ/mol) is observed for the third Al-O hydrolysis and via an equatorial substitution. Moreover, one can observe (table 1) that for a given step, over all frameworks and sites considered, the barrier spread (last row, table 1) show that the first step exhibits the lower variation across different frameworks and crystallographic position.

Table 1. Energy barriers $E^{\ddagger}$ (kJ/mol) and apparent barriers E_{app} (kJ/mol) for different numbers of water molecules and most probable mechanism[a] for each zeolite and T site studied. EFAL location and stabilities (kJ/mol) are also given.

Zeolite (T site)	**T site configuration[b]**	**$E^{\ddagger}$[c]**			**E_{app}[c]**			**EFAL location**	**EFAL stability**
		n=1	n=2	n=3	n=1	n=2	n=3		
CHA (T1O3)	4MR (chabazite cage)	76 ax	**114 ax**	61	21	**49**	-2	chabazite cage	-74
MOR (T4O4)	4MR (12MR)	**100** ax	94 eq	85 eq	**33**	27	32	12MR channel	-68
MFI (T3O4)	5MR (intersection)	**86** ax	65 eq	70 eq	16	11	**26**	straight channel	-117
MFI (T11O3)	5MR(straight ch.)	101 ax	84 eq	**114** eq	34	-13	**43**	Intersection	-136
MFI (T10O2)	4MR (sinusoidal ch.)	120 ax	37 eq	**161** eq	61	38	**78**	sinusoidal channel	-107
FAU (T1O1)	4MR (hexagonal prism)	98 ax	**100** ax	94 eq	35	**70**	-1	sodalite cage	-114
FAU (T1O3)	4MR (hexagonal prism)	83 ax	98 eq	**102** eq	29	**35**	22	supercage	-60
Barrier spread[d]	All sites	44	77	100	45	83	80	-	-

[a]Mechanism: ax and eq refer to axial and equatorial substitutions; [b]T site configuration: first value - smallest building unit to which the site belongs; brackets - location in zeolitic framework; [c] Bold – highest barrier for a given site. [d] Difference between highest and lowest values for the all column.

Assuming kinetic order 1 with respect to gaseous water, one may also consider apparent barriers, defined, for each step, according to equation (2).

$$E_{app}(nH_2O) = E^{\ddagger}(nH_2O) + \Delta E(I0(nH_2O)) - \Delta E(I2((n-1)H_2O)) \quad (2)$$

The values are reported in table 1, for each step of the reaction. For a given site, the highest apparent barrier is found for the first step (n=1) only for mordenite. The second (FAU, CHA) or third (MFI) steps are generally the most demanding from an apparent barriers point of view. The scattering of the highest apparent energy barriers is wider within a framework (26 to 78 kJ.mol^{-1} for MFI) than from a framework to the other (26 to 49 kJ.mol^{-1}, considering the most reactive site of each zeolite).

Whether one should consider or not consider apparent barriers will however depend on reactions orders, which cannot be easily solved by DFT calculations only. As a perspective of this work, one can suggest to undertake a full kinetic simulation of the process, based on calculated activation enthalpies and entropies for individual steps followed by a microkinetic model, in order to conclude, such as the one undertaken in ref. [51, 67].

3.2. Brønsted-Evans-Polanyi relationships for the hydrolysis of Al-O bonds

One key factor for controlling the rate of an elementary chemical reaction is its (free) energy barrier. While the evaluation of reaction energies provides insights about the stability of occurring products and intermediates along the reaction path, only the explicit determination of transition structures, allow us to determine the preferred pathway. However, the determination of transition structures is a demanding task and requires substantial amounts of computer time. If for a set of given reactions, a linear relationship between the energy barrier $E^{\ddagger}$ and the corresponding reaction energy ΔE_{react} exists, as postulated by the Brønsted-Evans-Polanyi principle,[68, 69] once knowing the reaction energy, the corresponding reaction barrier can be determined without its explicit calculation.

Figure 8 shows such a behavior for each of the three Al-O bond hydrolyses leading to the formation of an EFAL, as it was already reported for the very first Al-O bond breaking in our previous work.[49] The correlation coefficient for the first Al-O bond breaking is R^2=0.96 which allows an accurate determination of the reaction barrier by simply evaluating ΔE. This is also reflected in the box plot analyses shown in Supporting Information S4. For the first Al-O hydrolysis the interval of the reaction energy varies between 75 to 120 kJ/mol with a mean absolute error (MAE) of 2.4 kJ/mol and a maximum error (MAX) of 4.3 kJ/mol. This observation holds also true for the second Al-O hydrolysis. However, the correlation tends to degrade as quantified by a lower R^2 value of 0.90. The box plot analysis also shows a higher

fluctuation of the energy barriers varying between 37 to 114 kJ/mol. A reasonable MAE of 5.4 kJ/mol still allows accurate prediction of reaction barriers on the basis of reaction energies. However, a MAX of 14 kJ/mol due to the heterogeneity in interaction of the EFAL-precursor with the zeolitic framework and the successive creation of a silanol nest, displays the difficulty in predicting accurate trends from thermodynamics at this step. This difficulty is even more pronounced for the third Al-O bond hydrolysis (R^2= 0.49, MAE: 14 kJ/mol, MAX: 38 kJ/mol), for which the correlation cannot be considered as reliable anymore.

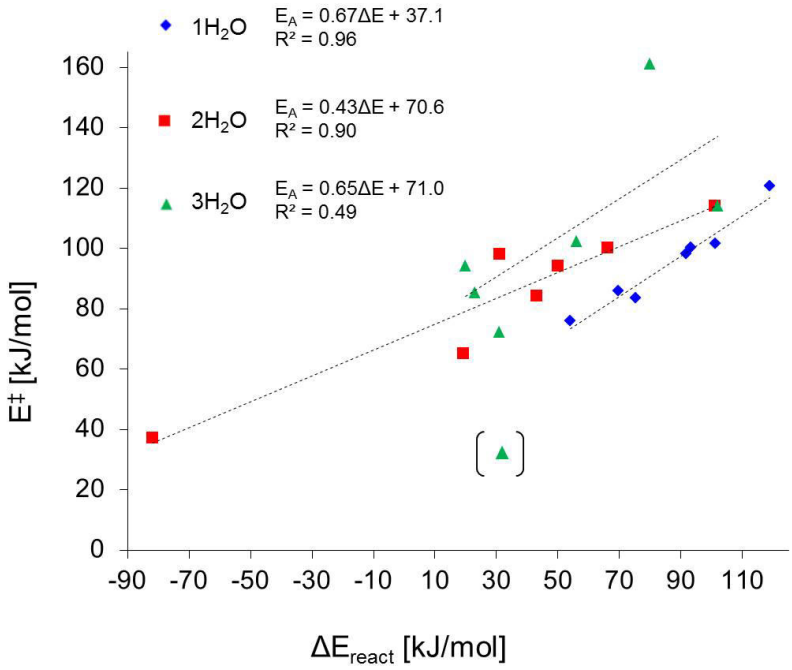

Figure 8. Plot of the energy barrier ($E^{\ddagger}$) as a function of the reaction energy (ΔE_{react}) for Al-O hydrolysis reactions occurring in zeolites (green triangle in brackets removed from correlation due to different hydrolysis mechanism; see text). The green triangle in brackets for third water molecules corresponds to the T1O3 site in H-CHA, which showed a specific mechanism for the third Al-O hydrolysis via EFAL precursor rotation with a subsequent concerted proton jump, was removed from the correlation.

This degradation is explained by the increasing amount of local and non-local effects which remain hard to predict from the simple knowledge of the thermodynamic data on reactant and product only. Thus, the parameters making it difficult to derive quantitative structure-activity relationships are the following ones:

- local structural constrains impacting the flexibility of the Al atoms,

- hydrogen bonds between the hydroxyl groups of the EFAL-precursor and the oxygen atoms of the zeolites walls, as well as the complex hydrogen bond network established after the formation of a silanol nest,
- evolution of the van der Waals contribution (confinement effect) in the course of dealumination and depending strongly on the zeolite.

With increasing number of Al-O bonds being broken, the amount of hydroxyl groups on the EFAL precursor as well as the number of silanols around the extracted Al atom increases, inducing a different hydrogen bond network. In addition, this trend depends not only on each T site's local environment but also on each intermediate involved in the BEP relationship. Comparison of the three slopes shows that the first (slope = 0.7) and third (slope = 0.6) Al-O hydrolysis transition structures exhibit the same sensitivity with regards to the stability of the intermediates, whereas the second Al-O bond hydrolysis (slope = 0.4) exhibits lower variations. However, there is no general trend regarding the rate determining step, as previously discussed (Table 1).

3.3. Thermodynamic considerations on the confinement effect on EFAL species

Additionally to their strong Brønsted acidity, zeolites are well known to possess properties such as shape selectivity, selective adsorption and diffusion, resulting from their microporous networks and curvature of their internal surfaces. The interactions between the zeolite framework and guest molecules (reactant, product, intermediates and TS) located within the cavities and channels are often of non-covalent nature. This confinement effect is an ubiquitous characteristic of zeolites.[18, 70-72] As indicated in the Methods part, we have taken into consideration the dispersion contribution for the whole dealumination mechanisms. In what follows, we would like to give a more detailed analysis of the confinement effects resulting from van der Waals interactions and acting on the EFAL product.

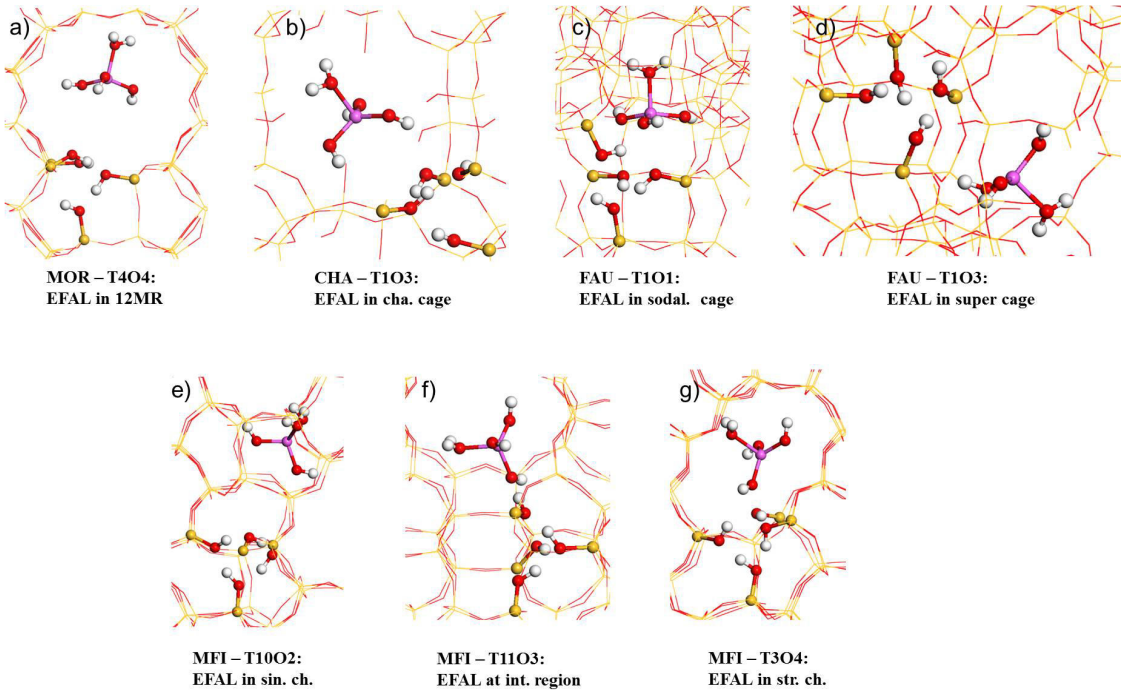

Figure 9. EFAL $Al(OH)_3H_2O$ upon dealumination of a) MOR, b) CHA, d), e) FAU and e)-g) MFI type zeolite located within the different channel systems (pink: Al; red: Si; yellow: O; pink: Al; white: H).

After the extraction of aluminum from a framework to a non-framework position as an EFAL species $Al(OH)_3H_2O$, and depending of its previous T site location, it can reside in different cavities present in the zeolitic framework (figure 9). Since each cavity has its own topology and curvature (e.g. the sodalite cage of FAU is spherically closed whereas the 12MR channel of MOR is opened along the c axis) exerting specific confinement effect on the residing EFAL species, this will affect its stability. The confinement effect can in turn be seen as a thermodynamic driving force for aluminum displacement from a framework to a non-framework position.

Figure 10 reports the interaction energy of the EFAL species $Al(OH)_3H_2O$ with the zeolite cavity (using the zeolite and 4 water molecules as reference) as a function of the cavity diameter d according to ref. [73]. Numerical values are also reported in Table 1. The curve reflects that for to small cavities, e.g. the hexagonal prism ($d < 4$ Å) present in zeolite Faujasite, the Pauli repulsion destabilizes the residence of an EFAL species in such a confined surrounding. On the other hand, for very large pores, like for instance present in Chabazite or

in the FAU supercage (d > 8 Å), a weak confinement effect from the zeolitic framework is expected. As a result of this analysis, the highest stabilization of $Al(OH)_3H_2O$ was found in the intersection region between sinusoidal and straight channels of MFI zeolite (d = 6-8 Å).

This analysis shows that complementary to the kinetic values of the dealumination mechanisms detailed before (Table 1), the formation of EFAL species can also be influenced by the confinement effect induced by the pore topology. For instance, in FAU where T1O1 and T1O3 sites exhibit very similar energy barriers for the limiting step (~100 kJ/mol), the driving force may be the higher thermodynamic stability of EFAL formed in the sodalite cage from T1O1. In MFI, kinetic and thermodynamic data are converging and the most favored site for the first EFAL formation is T3O4 at the intersection of sinusoidal and straight channels.

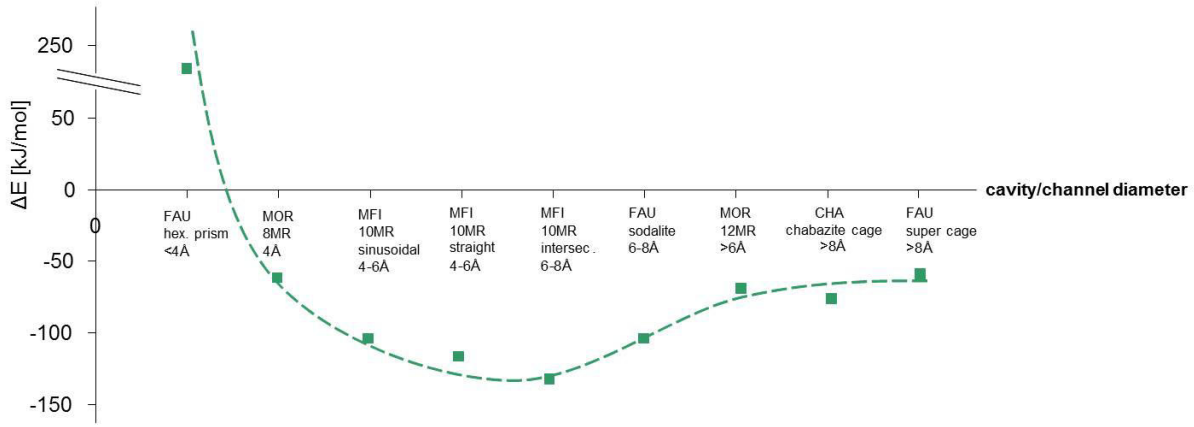

Figure 10. Qualitative plotting of EFAL $Al(OH)_3H_2O$ stability (using the zeolite and 4 water molecules as reference) as a function of the channel and cavity diameter of the zeolitic frameworks MOR, FAU, CHA and MFI. FAU hexagonal prismatic cage and MOR 8MR, are added to provide additional examples (not treated before) illustrating EFAL configuration in constrained cavity.

5. Discussion

From the very first stage of the reaction, we propose pentahedral or distorted tetrahedral Al atom as relevant intermediates for the formation of EFAL. Such Al species were identified experimentally and are supposed to be at the initiation of aluminum dislodgement to extra-framework positions.[28, 31] Contrary to the general opinion on

dealumination upon steam treatment, Agostini *et al.* showed on steamed zeolite Y – FAU framework , by in situ XAS and XRPD measurements, that a structural deformation already occurs at moderate temperatures (450 – 500 K) when the first water molecules start to repopulate the pores.[28] This result seems to be consistent with the moderate energy barriers (~100 kJ/mol) found for our investigated T sites in FAU. In contrast, energy barriers as provided by Swang et al.[46, 47] (in the case of CHA, however) seem to be too high to be compatible with such studies which raises questions about their proposed mechanism. Considering apparent barriers, they obtain for n=1 ~125 $kJ.mol^{-1}$, much higher than all values reported in the present paper. Note the same authors agree with our proposal, by considering mechanisms similar to ours for SAPO-34 desilication.[50, 51]

By combination of our mechanistic investigation of the dealumination with the confinement effect found for the residence of EFAL species inside the cavities we are able to elucidate experimental results regarding Faujasite. Agostini *et al.* showed the appearance of a fraction 30-35% of the total Al in the sodalite cage.[28] Analyzing Figures 7 and 10, this can be explained only by including thermodynamic considerations because all reaction barriers are in the range of about 100 kJ/mol. Apparent barriers even suggest better kinetics for EFAL formation in the supercage (E_{app} = 35 $kJ.mol^{-1}$ for T1O3 versus 70 for EFAL formation in the sodalite cage, T101). Indeed, the formation of an EFAL residing in the supercage is thermodynamically less favored than its presence in the sodalite cage. Moreover, along the reaction path, the most stable structure for the T1O1 site (giving rise to the EFAL in the sodalite cage) is I0($4H_2O$) (ΔE = - 111 kJ/mol) compared to I0($1H_2O$) (ΔE = - 63 kJ/mol) explaining that this site is more stable when extracted from the framework. This assumption holds not true for T1O3 (giving rise to EFAL in the supercage) since the most stable structure along the reaction path was identified for I0($3H_2O$) (ΔE = - 128 kJ/mol) showing that only partial dealumination has occurred with formation of a stable penta-coordinated Al species

not being an extra-framework species. So both the relative stability of intermediates and final products are driving forces for the regioselectivity of EFAL formation in FAU, rather than barriers.

At the mesoscale, employing FIB and SEM analyzes Karwacki *et al.* revealed an architecture-dependent mesopore formation upon steaming of ZSM-5 zeolite: sinusoidal channels were more affected by the dealumination than straight channels.[32] Upon analysis of the reaction path of T sites located in the sinusoidal channels (T10O2), straight channels (T11O3) and the intersection regions (T3O4) (Figure 5), we confirm this regioselectivity and we determine that the intersection region of sinusoidal and straight channels is the place where the dealumination of T3O4 is the most favored in terms of both kinetics and thermodynamics. At this site, the tetrahedral Al atom is more stable in a non-framework position dictated by the stability of all intermediates (but one) and driven by the confinement effect of the intersection region. The T site in the sinusoidal channel shows the highest energy barriers in the series of these three T sites and moreover the most stable structure along the reaction path was found for I0($3H_2O$) (ΔE = - 140 kJ/mol) meaning that at T10O2 Al is more stable as a framework species. The same observation holds also true for the T11O3 site where the most stable structure was I0($3H_2O$) (ΔE = -106 kJ/mol). However experimentally, no information is available for the initiation site for dealumination provided in the present study. So our result combined with experimental would indicate that once the dealumination has been initiated at the intersection, the propagation of mesopores occurs along sinusoidal channels. Understanding more precisely the origins of this behavior would require additional investigations, such as the simulation of the propagation of extra-framework formation, up to the mesopore. A first tentative explanation can be provided looking at the results reported in Figure 8. Indeed, EFAL is the less stabilized in the sinusoidal channel, whereas it is preferentially located at the intersection, and in the straight channel. We can also suggest that

pore blocking inside the straight channels occurs. After most intersection sites have been dealuminated, the corresponding EFAL diffuses preferentially in the straight channels, where they are also stabilized, preventing their further dealumination and promoting the formation of mesopores along sinusoidal channels.

5. Conclusions

The present study reports a mechanistic investigation of dealumination reactions on 8 BAS belonging to four zeolitic frameworks: MOR, MFI, FAU and CHA. We demonstrated that the very first step in the initiation of the dealumination of a given T site, is a water adsorption on Al in anti-position to the Brønsted acid site, leading to the formation of a pentahedral or distorted tetrahedral Al atom. In a subsequent step, the first Al-O hydrolysis takes place via a 1,2-dissociation of a water molecule with axial substitution of the silanol. This mechanism is the same for each T site, regarding the reaction of the first water molecule. We show that once the first Al-O bond is broken and the Al atom becomes more flexible in terms of structural changes, alternative pathways are possible, due to a set of effects (i.e. hydrogen bond network between the EFAL precursor and the zeolitic walls as well as the resulting silanol nest, and van der Waals contributions also linked with confinement effects) affecting the stability of TS and intermediates along the path. In particular, the occurrence of 1,2-dissociation of water with equatorial (instead of axial) substitution of Si-OH becomes competitive. Brønsted-Evans-Polanyi relationships for each Al-O hydrolysis have been established but they reveal a strong degradation for the third Al-O hydrolysis due to these complex local and non-local effects.

Moreover, we show that the very first Al-O bond breaking step is kinetically determining for the formation of EFAL in MOR and one site (T3O4) of MFI. For other sites, the subsequent Al-O bond breaking steps may become rate limiting. By considering apparent

barriers instead of energy barriers, the first Al-O bond breaking appears to be limiting in the case of MOR only.

Last but not least, we quantified the thermodynamic stability of EFAL species formed in the same zeolites cavities and channel systems. We established a direct link with the confinement effect exerted by zeolites as a function of the cavity diameter of the micropores where the EFAL is located. Aside the kinetic effects, we show that this thermodynamic stability may represent a complementary driving force for Al dislodgement to extra-framework positions, in particular in FAU. The combination of kinetic and thermodynamic of EFAL formation is likely to explain some experimental features regarding the regioselectivity of the formation of EFALs.

Acknowledgements: All calculations were performed at IFPEN HPC centre and at IDRIS/CINES HPC centres within projects x2014086134 and x2015086134 funded by GENCI.

References

[1] W.O. Haag, R.M. Lago, P.B. Weisz, Nature 309 (1984) 589-591.
[2] M. Boronat, A. Corma, Catal. Lett. 145 (2015) 162-172.
[3] C. Marcilly, Acido-Basic Catalysis - Application to Refining and Petrochemistry, in: Acido-Basic Catalysis - Application to Refining and Petrochemistry, Editions TECHNIP, 2005.
[4] A. Corma, Chem. Rev. 95 (1995) 559-614.
[5] K.P. de Jong, J. Zečević, H. Friedrich, P.E. de Jongh, M. Bulut, S. van Donk, R. Kenmogne, A. Finiels, V. Hulea, F. Fajula, Ang. Chem., Int. Ed. 122 (2010) 10272-10276.
[6] W. Vermeiren, J.P. Gilson, Top. Catal. 52 (2009) 1131-1161.
[7] G. Busca, Chem. Rev. 107 (2007) 5366-5410.
[8] S. Mitchell, N.-L. Michels, K. Kunze, J. Pérez-Ramírez, Nature Chem. 4 (2012) 825-831.
[9] V. Valtchev, G. Majano, S. Mintova, J. Perez-Ramirez, Chem. Soc. Rev. 42 (2013) 263-290.
[10] C.H. Christensen, K. Johannsen, I. Schmidt, C.H. Christensen, J. Am. Chem. Soc. 125 (2003) 13370-13371.
[11] J.C. Groen, T. Bach, U. Ziese, A.M. Paulaime-van Donk, K.P. de Jong, J.A. Moulijn, J. Perez-Ramirez, J. Am. Chem. Soc. 127 (2005) 10792-10793.
[12] K. Na, C. Jo, J. Kim, K. Cho, J. Jung, Y. Seo, R.J. Messinger, B.F. Chmelka, R. Ryoo, Science 333 (2011) 328-332.
[13] M. Hartmann, Angew. Chem. Int. Ed. 43 (2004) 5880-5882.
[14] W.J. Roth, O.V. Shvets, M. Shamzhy, P. Chlubna, M. Kubu, P. Nachtigall, J. Cejka, J. Am. Chem. Soc. 133 (2011) 6130-6133.
[15] M. Milina, S. Mitchell, D. Cooke, P. Crivelli, J. Perez-Ramirez, Angew. Chem. Int. Ed. 54 (2015) 1591-1594.
[16] M. Milina, S. Mitchell, P. Crivelli, D. Cooke, J. Pérez-Ramírez, Nature Communications (2014).
[17] M. Moliner, C. Martinez, A. Corma, Angew. Chem. Int. Ed. 54 (2015) 2-22.
[18] E.G. Derouane, J.M. Andre, A.A. Lucas, J. Catal. 110 (1988) 58-73.
[19] B. Smit, T.L.M. Maesen, Chem. Rev. 108 (2008) 4125-4184.
[20] S. van Donk, A.H. Janssen, J.H. Bitter, K.P. de Jong, Catal. Rev. 45 (2003) 297-319.
[21] M.-C. Silaghi, C. Chizallet, P. Raybaud, Microporous Mesoporous Mater. 191 (2014) 82-96.
[22] S. Bordiga, P. Ugliengo, A. Damin, C. Lamberti, G. Spoto, A. Zecchina, G. Spanò, R. Buzzoni, L. Dalloro, F. Rivetti, Top. Catal. 15 (2001) 43-52.
[23] J.i. Dědeček, S. Sklenak, C. Li, F. Gao, J.i. Brus, Q. Zhu, T. Tatsumi, J. Phys. Chem. C 113 (2009) 14454-14466.
[24] E. Senderov, I. Halasz, D.H. Olson, Mic. Mes. Mat. 186 (2014) 94-100.
[25] I. Halasz, E. Senderov, D.H. Olson, J.-J. Liang, J. Phys. Chem. C 119 (2015) 8619-8625.
[26] C.R.A. Catlow, P.S. Baram, S.C. Parker, J. Purton, K.V. Wright, Radiat. Eff. Defects Solids 134 (1995) 57-64.
[27] B.H. Wouters, T.H. Chen, P.J. Grobet, J. Am. Chem. Soc. 120 (1998) 11419-11425.
[28] G. Agostini, C. Lamberti, L. Palin, M. Milanesio, N. Danilina, B. Xu, M. Janousch, J.a. van Bokhoven, J. Am. Chem. Soc. 132 (2010) 667-678.
[29] L. Benco, T. Demuth, J. Hafner, F. Hutschka, H. Toulhoat, J. Catal. 209 (2002) 480-488.
[30] D.L. Bhering, A. Ramirez-Solis, C.J.A. Mota, J. Phys. Chem. B 107 (2003) 4342-4347.
[31] T.-H. Chen, K. Houthoofd, P.J. Grobet, Microporous Mesoporous Mater. 86 (2005) 31-37.

[32] L. Karwacki, D.A.M. de Winter, L.R. Aramburo, M.N. Lebbink, J.A. Post, M.R. Drury, B.M. Weckhuysen, Angew. Chem. Int. Ed. 50 (2011) 1294-1298.
[33] S. Li, A. Zheng, Y. Su, H. Zhang, L. Chen, J. Yang, C. Ye, F. Deng, J. Am. Chem. Soc. 129 (2007) 11161-11171.
[34] O. Lisboa, M. Sánchez, F. Ruette, J. Mol. Catal. A 294 (2008) 93-101.
[35] N. Malicki, G. Mali, A.-A. Quoineaud, P. Bourges, L.J. Simon, F. Thibault-Starzyk, C. Fernandez, Microporous Mesoporous Mater. 129 (2010) 100-105.
[36] M. Müller, G. Harvey, R. Prins, Microporous Mesoporous Mater. 34 (2000) 135-147.
[37] P.C. Van Geem, K.F.M.G.J. Scholle, G.P.M. Van der Velden, W.S. Veeman, J. Phys. Chem. 92 (1988) 1585-1589.
[38] R.A. Beyerlein, C. Choi-Feng, J.B. Hall, B.J. Huggins, G.J. Ray, Topics Catal. 4 (1997) 27-42.
[39] J.A. van Bokhoven, D.C. Koningsberger, P. Kunkeler, H. van Bekkum, A.P.M. Kentgens, J. Am. Chem. Soc. 122 (2000) 12842-12847.
[40] L.R. Aramburo, L. Karwacki, P. Cubillas, S. Asahina, D.A.M. de Winter, M.R. Drury, I.L.C. Buurmans, E. Stavitski, D. Mores, M. Daturi, P. Bazin, P. Dumas, F. Thibault-Starzyk, J.A. Post, M.W. Anderson, O. Terasaki, B.M. Weckhuysen, Chem. Eur. J. 17 (2011) 13773-13781.
[41] J.M. Ruiz, M.H. McAdon, J.M. Garcés, J. Phys. Chem. B 101 (1997) 1733-1744.
[42] C.J.A. Mota, D.L. Bhering, N. Rosenbach, Angew. Chem. Int. Ed. 43 (2004) 3050-3053.
[43] L. Benco, T. Bucko, J. Hafner, H. Toulhoat, J. Phys. Chem. B 108 (2004) 13656-13666.
[44] G. Ricchiardi, A. de Man, J. Sauer, Phys. Chem. Chem. Phys. 2 (2000) 2195-2204.
[45] J. To, A.A. Sokol, S.A. French, C.R.A. Catlow, P. Sherwood, H.J.J. van Dam, Angew. Chem. Int. Ed. 45 (2006) 1633 –1638.
[46] S. Malola, S. Svelle, F.L. Bleken, O. Swang, Angew. Chem. Int. Ed. 51 (2012) 652-655.
[47] T. Fjermestad, S. Svelle, O. Swang, J. Phys. Chem. C 117 (2013) 13442-13451.
[48] S. Grimme, J. Comput. Chem. 27 (2006) 1787-1799.
[49] M.-C. Silaghi, C. Chizallet, E. Petracovschi, T. Kerber, J. Sauer, P. Raybaud, ACS Catalysis 5 (2015) 11-15.
[50] T. Fjermestad, S. Svelle, O. Swang, J. Phys. Chem. C 119 (2015) 2073-2085.
[51] T. Fjermestad, S. Svelle, O. Swang, J. Phys. Chem. C 119 (2015) 2086-2095.
[52] G. Kresse, J. Hafner, Phys. Rev. B 49 (1994) 14251-14269.
[53] G. Kresse, J. Non-Cryst. Solids 192–193 (1995) 222-229.
[54] G. Kresse, J. Furthmüller, Comput. Mat. Sci. 6 (1996) 15-50.
[55] G. Kresse, D. Joubert, Phys. Rev. B 59 (1999) 1758-1775.
[56] J.P. Perdew, K. Burke, M. Ernzerhof, Phys. Rev. Lett. 77 (1996) 3865-3868.
[57] C. Tuma, J. Sauer, Phys. Chem. Chem. Phys. 8 (2006) 3955-3965.
[58] C. Tuma, J. Sauer, Chem. Phys. Lett. 387 (2004) 388-394.
[59] J. Van der Mynsbrugge, K. Hemelsoet, M. Vandichel, M. Waroquier, V. Van Speybroeck, J. Phys. Chem. C 116 (2012) 5499-5508.
[60] F. Göltl, A. Grüneis, T. Bucko, J. Hafner, J. Chem. Phys. 137 (2012) 114111.
[61] W. E, W. Ren, E. Vanden-Eijnden, Phys. Rev. B 66 (2002) 052301.
[62] P. Fleurat-Lessard, P. Dayal, Code freely available at: http://perso.ens-lyon.fr/paul.fleurat-lessard/ReactionPath.htm, accessed 10th January 2012.
[63] G. Henkelman, H. Jonsson, J. Chem. Phys. 113 (2000) 9978-9985.
[64] P. Pulay, Chem. Phys. Lett. 73 (1980) 393-398.
[65] A. Heyden, A.T. Bell, F.J. Keil, J. Chem. Phys. 123 (2005) 224101.
[66] M. Czjzek, H. Jobic, A.N. Fitch, T. Vogt, J. Phys. Chem. 96 (1992) 1535-1540.
[67] T. Fjermestad, S. Svelle, O. Swang, J. Phys. Chem. C 119 (2015) 20782−20782.
[68] J.N. Brønsted, Chem. Rev. 5 (1928) 231-338.

[69] M.G. Evans, M. Polanyi, Trans. Farad. Soc. 34 (1938) 11-24.
[70] D. Barthomeuf, Mater. Chem. Phys. 17 (1987) 49-71.
[71] J. Sauer, P. Ugliengo, E. Garrone, V.R. Saunders, Chem. Rev. 94 (1994) 2095.
[72] J. Sauer, R. Zahradník, Int. J. Quantum Chem. 26 (1984) 793-822.
[73] E.L. First, C.E. Gounaris, J. Wei, C.A. Floudas, Phys. Chem. Chem. Phys. 13 (2011) 17339-17358.